Exact Analysis of RIS-Aided THz Wireless Systems Over α-μ Fading With Pointing Errors

Vinay Kumar Chapala, *Graduate Student Member, IEEE*, and S. M. Zafaruddin, *Senior Member, IEEE*

***Abstract*— Reconfigurable intelligent surfaces (RIS) can have an excellent use case for terahertz (THz) wireless transmissions. In this letter, we analyze the performance of a RIS-empowered THz system over the combined effect of α-μ fading and pointing errors. We derive exact closed-form expressions of density and distribution functions of the resultant signal-to-noise ratio (SNR) considering an independent and not identically distributed (i.ni.d.) channel model. Using the derived statistical results, we present an exact analysis on outage probability, ergodic capacity, and average bit-error-rate (BER) of the considered system. We also develop asymptotic analysis on the outage probability and average BER to derive diversity order in terms of system parameters. The proposed analysis provides insights to mitigate the effect of pointing errors and shows that the RIS can significantly improve the performance of THz communications. We validate the analytical results using numerical and Monte Carlo simulations and demonstrate the scaling of system performance with an increase in the number of RIS elements.**

***Index Terms*— Bit error rate, ergodic rate, Fox's H function, outage probability, reconfigurable intelligent surface, terahertz.**

I. Introduction

MODERN wireless systems are designed based on the principle that channel environments cannot be controlled. Reconfigurable intelligent surfaces (RIS) are emerging as a potential technology to steer the signal propagation in the desired direction for enhanced performance in next-generation wireless systems [1]–[3]. On the other hand, the terahertz (0.3 THz to 10 THz) spectrum is the next frontier in wireless communications providing tremendously high bandwidth for data transmissions [4], [5]. The RIS can be more promising to overcome high attenuation by creating a virtual line-of-sight (LOS) path in a cost-efficient manner for THz wireless transmissions. The envisioned RIS technology combined with THz transmission has a huge potential to revolutionize the design of 6G wireless networks.

The performance of RIS systems has been analyzed for various wireless fading channels over radio-frequency (RF) transmissions [6]–[16]. Recently, the use of the THz spectrum for wireless communications has sparked research interests in the last few years [17]–[22]. However, in contrast to the RF transmissions, the THz link suffers from transceiver impairments and random pointing errors due to the misalignment between transmitter and receiver antenna beam at higher frequencies. Moreover, the path-loss in the THz band is higher due to molecular absorption of the signal at extremely small wavelengths providing an excellent use case for the RIS. In [18], RIS-assisted THz transmission was studied without considering the effect of short-term fading and pointing errors. A deep reinforcement learning (DRL) based multi-hop RIS-empowered THz system was proposed in [19]. The authors in [20] provided an analytical framework for RIS-aided THz communications by deriving outage probability and ergodic capacity over fluctuating two rays (FTR) channel model combined with antenna misalignment and hardware impairments. The authors in [14] employed the method of moment generating function (MGF) to derive the exact expression for the outage probability of RIS-aided millimeter-wave communications over the FTR fading model. It should be noted that the FTR model consists of an infinite sum to generate the probability distribution function (PDF) and cumulative distribution function (CDF), which approximates the system performance when a finite number of terms are used for the convergence of distribution functions. Recently, the authors in [21], [22] considered the generalized α-μ fading to analyze the performance of THz communications. The α-μ is a generalized model that includes other fading models such as Rayleigh and Nakagami-m as a particular case. In [15], the authors analyzed the effective rate of RIS-assisted communications by approximating the sum of cascaded α-μ distributed random variables with the mixture of Gaussian without considering pointing errors. In [16], the authors presented exact expressions of the outage probability and ergodic capacity for a RIS-assisted system without pointing errors over generalized Fox's H fading channels, which contains α-μ, as a particular case. To the best of authors' knowledge, a performance analysis of the RIS system over α-μ fading with pointing errors for THz transmissions is not available in the related literature. A recent measurement campaign validates α-μ for small-scale fading in THz wireless systems [23].

In this letter, we analyze the performance of a RIS-empowered THz wireless system by deriving exact closed-form expressions of PDF and CDF of the effective fading channel under the combined effect of independent and not identically distributed (i.ni.d.) α-μ fading and zero-boresight pointing errors. Using the derived PDF and CDF, we present an exact analysis of outage probability, ergodic capacity, and average bit-error-rate (BER) of the considered system in terms of Fox's H function. We also develop asymptotic analysis on the outage probability and average BER in terms of Gamma function. We derive the diversity order of the system depicting performance improvement with an increase in the RIS elements and providing design specifications to mitigate the effect of pointing errors. We validate the analytical results using numerical analysis and Monte Carlo simulations demonstrating the impact of channel

Manuscript received July 10, 2021; revised August 9, 2021; accepted August 30, 2021. Date of publication September 7, 2021; date of current version November 11, 2021. This work was supported in part by the Science and Engineering Research Board (SERB), Department of Science and Technology (DST), Government of India, under Start-Up Research Grant SRG/2019/002345. The associate editor coordinating the review of this letter and approving it for publication was G. C. Alexandropoulos. *(Corresponding author: Vinay Kumar Chapala.)*

The authors are with the Department of Electrical and Electronics Engineering, Birla Institute of Technology and Science Pilani, Pilani, Rajasthan 333031, India (e-mail: p20200110@pilani.bits-pilani.ac.in; syed.zafaruddin@pilani.bits-pilani.ac.in).

Digital Object Identifier 10.1109/LCOMM.2021.3110865

fading and the number of RIS elements on THz wireless transmissions.

II. System Model

We consider a transmission model, where a source communicates with a destination through an N-element RIS operating in the THz band. We consider that the elements of RIS are spaced half of the wavelength and assume independent channels at the RIS [2], [14], [18]. We ignore the direct link between the source and destination, which is a reasonable assumption for THz transmissions owing to higher path loss [20]. Even for the RF transmissions, the direct link is ignored in many research works (see [14]–[16] and references therein). Assuming flat fading and perfect knowledge of channel phase at each RIS element, the signal received at the destination through RIS is given as [24]

$$y = h_l \sum_{i=1}^{N} |h_i||g_i|(s + w_t) + w_r + w \tag{1}$$

where h_l is the path gain from the source to the destination through RIS, $|h_i|$ and $|g_i|$ are channel fading coefficients between the source to the i-th RIS element and between the i-th RIS element to the destination, respectively, s is the transmitted signal with power P, and w is the additive Gaussian noise with variance σ_w^2. Here $w_t \sim \mathcal{CN}(0, k_t^2 P)$, and $w_r \sim \mathcal{CN}(0, k_r^2 P |h_l| \sum_{i=1}^{N} |h_i||g_i||^2)$ denote hardware impairments with factor k_t and k_r, which characterizes the extent of hardware imperfections in the transmitter and receiver, respectively.

The path loss of the cascaded link can be modeled using the free-space channel modeling of RIS-assisted communications with molecular absorption losses at THz bands [18], [20], [25]. We assume short-term fading coefficients $|h_i|$ and $|g_i|$ to be independent but non-identical distributed according to the combined effect of α-μ fading and pointing errors [21]:

$$f_{|h_i|}(x) = \psi_i x^{\phi_i - 1} \times \Gamma\left(\mu_i - \frac{\phi_i}{\alpha_i}, \zeta_i x^{\alpha_i}\right) \tag{2}$$

where $\psi_i = \phi_i S_i^{-\phi_i} \frac{\mu_i^{\phi_i/\alpha_i}}{\Omega_i^{\phi_i}\Gamma(\mu_i)}$, and $\zeta_i = \frac{\mu_i}{\Omega^{\alpha_i}} S_i^{-\alpha_i}$. Here, α_i and μ_i are fading parameters that provide flexibility to model various channel conditions, whereas S_i and ϕ_i denote pointing error parameters. The term S_i denotes the fraction of the collected power when both the antennas are fully aligned and ϕ_i denotes the ratio of normalized beam-width to the jitter. Note that under the scenario of correlated channels at the RIS, a generalized Gamma fading model with arbitrary correlation can be used [26].

III. Statistical Analysis

To facilitate performance analysis, the distribution function of $\sum_{i=1}^{N} |h_i||g_i|$ is required. Considering L reflecting paths in each RIS element, we derive the PDF and CDF of the generalized system $Z = \sum_{i=1}^{N} Z_i$, where $Z_i = \prod_{j=1}^{L} |x_{i,j}|$ and $x_{i,j}, j = 1, 2, \cdots L$ are i.ni.d random variable distributed according to (2). We denote $\{a_i\}_1^N = \{a_1, \cdots, a_N\}$ and imaginary number by $\jmath$.

Proposition 1: If $x_{i,j}$ are i.ni.d random variables and distributed according to (2)*, then the MGF of $Z_i = \prod_{j=1}^{L} |x_{i,j}|$ is given as*

$$M_{Z_i}(s) = \Big(\prod_{j=1}^{L} \psi_j \zeta_j^{-\frac{\phi_j}{\alpha_j}}\Big) H_{L+1,2L}^{2L,1}\left[\frac{1}{s}\prod_{j=1}^{L}\zeta_j^{\frac{1}{\alpha_j}}\middle|\begin{matrix} V_1 \\ V_2 \end{matrix}\right] \tag{3}$$

where $V_1 = (1,1), (1+\phi_1, 1), \cdots, (1+\phi_L+1)$, $V_2 = (\mu_1, \frac{1}{\alpha_1}), \cdots, (\mu_L, \frac{1}{\alpha_L}), (\phi_1, 1), \cdots, (\phi_L, 1)$ ϕ_j and S_j are pointing errors parameters, and α_j and μ_j are the fading parameters for $j = 1, 2, 3, \cdots, L$.

Proof: See Appendix A. ∎

Theorem 1: If $x_{i,j}$ are i.ni.d random variables and distributed according to (2) *and $Z_i = \prod_{j=1}^{L} |x_{i,j}|$, then the PDF and CDF of $Z = \sum_{i=1}^{N} Z_i$ are given as*

$$f_Z(z) = \Big(\frac{1}{z}\prod_{i=1}^{N}\prod_{j=1}^{L}\psi_{i,j}\zeta_{i,j}^{-\frac{\phi_{i,j}}{\alpha_{i,j}}}\Big) \times H_{0,1:L+1,2L;\cdots;L+1,2L}^{0,0:2L,1;\cdots;2L,1}\left[U(z)\middle|\begin{matrix} -:V_1 \\ (1;1,\cdots,1):V_2 \end{matrix}\right] \tag{4}$$

$$F_Z(z) = \Big(\prod_{i=1}^{N}\prod_{j=1}^{L}\psi_{i,j}\zeta_{i,j}^{-\frac{\phi_{i,j}}{\alpha_{i,j}}}\Big) \times H_{0,1:L+1,2L;\cdots;L+1,2L}^{0,0:2L,1;\cdots;2L,1}\left[U(z)\middle|\begin{matrix} -:V_1 \\ (0;1,\cdots,1):V_2 \end{matrix}\right] \tag{5}$$

where $U(z) = \{z\prod_{j=1}^{L}\zeta_{i,j}^{\frac{1}{\alpha_{i,j}}}\}_{i=1}^{N}$, $V_1 = \{(1,1), \{(1+\phi_{i,j}, 1)\}_1^L\}_{i=1}^N$, $V_2 = \{\{(\mu_{i,j}, \frac{1}{\alpha_{i,j}})\}_1^L, \{(\phi_{i,j}, 1)\}_1^L\}_{i=1}^N$ given in (4) and (5), respectively, where ϕ_j and S_j are pointing errors parameters, and α_j and μ_j are the fading parameters for $j = 1, 2, 3, \cdots, L$.

Proof: See Appendix B. ∎

It can be seen from Theorem 1 that Fox's H representation facilitates in deriving exact analysis and it is useful for insightful asymptotic behavior of the system performance.

IV. Performance Analysis

It can be easily seen that using $L = 2$ with $x_{i,1} = h_i$ and $x_{i,2} = g_i$ in Theorem 1 corresponds to the RIS-enabled system in (1). Thus, an expression for SNR is $\gamma = \frac{\gamma_0|h|^2}{k^2\gamma_0|h|^2+1}$, where $k^2 = k_t^2 + k_r^2$, $\gamma_0 = \frac{P|h_l|^2}{\sigma_w^2}$ and $h = \sum_{i=1}^{N}|h_i||g_i|$. A straightforward transformation of random variables with $L = 2$ in (4) and (5) leads to PDF $f_\gamma(\gamma)$ and CDF $F_\gamma(\gamma)$ of SNR as

$$f_\gamma(\gamma) = \frac{1}{2\big(1-\gamma k^2\big)^2\sqrt{\frac{\gamma_0\gamma}{1-\gamma k^2}}} f_Z\left(\sqrt{\frac{\gamma}{\gamma_0(1-\gamma k^2)}}\right) \tag{6}$$

$$F_\gamma(\gamma) = F_Z\left(\sqrt{\frac{\gamma}{\gamma_0(1-\gamma k^2)}}\right) \tag{7}$$

1) Outage Probability: The outage probability P_{out} is defined as the probability of failing to reach an SNR threshold value, γ_{th}. An exact expression for the outage probability is given as $P_{\text{out}} = Pr(\gamma \le \gamma_{\text{th}}) = F_\gamma(\gamma_{\text{th}})$. Further, we use [27] to derive the outage probability asymptotically (denoted by P_{out}^{∞}) at high SNR $\gamma_0 \to \infty$ in terms of Gamma function:

$$P_{\text{out}}^{\infty} = \prod_{i=1}^{N}\prod_{j=1}^{2}\psi_{i,j}\zeta_{i,j}^{-\frac{\phi_{i,j}}{\alpha_{i,j}}}\Big(\sqrt{\frac{\gamma_{th}}{\gamma_0(1-\gamma_{\text{th}}k^2)}}\Big)^{\prod_{j=1}^{2}\zeta_{i,j}^{\frac{1}{\alpha_{i,j}}}})^{p_i}\Gamma(p_i) \times \frac{\prod_{j=1,\mu_{i,j}\neq\frac{p_i}{\alpha_{i,j}}}^{2}\Gamma(\mu_{i,j}-\frac{p_i}{\alpha_{i,j}})\prod_{j=1,\phi_{i,j}\neq p_i}^{2}\Gamma(\phi_{i,j}-p_i)}{\Gamma(1+\sum_{i=1}^{N}p_i)\prod_{j=1}^{2}\Gamma(1+\phi_{i,j}-p_i)} \tag{8}$$

where $p_i = \min\{\alpha_{i,1}\mu_{i,1}, \phi_{i,1}, \alpha_{i,2}\mu_{i,2}, \phi_{i,2}\}$. In order to get the outage-diversity order G_{out} of the system, we express (8) as $P_{out}^{\infty} \propto \gamma_0^{-G_{\text{out}}}$ to get $G_{\text{out}} = \sum_{i=1}^{N} \min\{\frac{\alpha_{i,1}\mu_{i,1}}{2}, \frac{\phi_{i,1}}{2}, \frac{\alpha_{i,2}\mu_{i,2}}{2}, \frac{\phi_{i,2}}{2}\}$. The diversity order shows that the performance of the considered system improves with an increase in the number of RIS elements. Further, we simplify (8) for the i.i.d case with $\phi > \alpha\mu$ to get

$$P_{\text{out}}^{\infty} = \frac{1}{\Gamma(1+N\alpha\mu)} \times \Big(\big(\frac{\gamma_{\text{th}}}{\Omega^4 S^4 \gamma_0 (1-\gamma_{\text{th}} k^2)} \big)^{\frac{\alpha\mu}{2}} \frac{\alpha\phi^2 \mu^{2\mu} \Gamma(\alpha\mu)}{(\phi-\alpha\mu)^2 (\Gamma(\mu))^2} \Big)^N \quad (9)$$

It can be seen from (9) that an increase in RIS elements (i.e., N) improves the outage performance at high SNR.

2) Average BER: Denoting a and b as modulation specific constants, the average BER is [21]:

$$\bar{P}_e = a\sqrt{\frac{b}{4\pi}} \int_0^{\infty} e^{-b\gamma} \gamma^{-\frac{1}{2}} F_{\gamma}(\gamma) d\gamma \quad (10)$$

We substitute $F_{\gamma}(\gamma)$ from (7) with $k=0$ in (10), use the definition of Multivariate Fox's-H function, and interchange the order of integration to get

$$\bar{P}_e = (a\sqrt{\frac{b}{4\pi}}) \prod_{i=1}^{N} \prod_{j=1}^{2} \psi_{i,j} \zeta_{i,j}^{-\frac{\phi_{i,j}}{\alpha_{i,j}}} \Bigg[(\frac{1}{2\pi\jmath})^N \int_{\mathcal{L}} \Big(\sqrt{\gamma_0} \prod_{j=1}^{2} \zeta_{i,j}^{\frac{-1}{\alpha_{i,j}}} \Big)^{n_i} \times \prod_{j=1}^{2} \frac{\Gamma(\phi_{i,j}+n_i)}{\Gamma(\phi_{i,j}+n_i+1)} \prod_{j=1}^{2} \Gamma(\mu_{i,j} + \frac{n_i}{\alpha_{i,j}}) \times (\frac{\Gamma(-n_i)}{\Gamma(1-\sum_{i=1}^{N} n_i)}) \Big[\int_0^{\infty} \exp^{-b\gamma} \gamma^{-\frac{1}{2} - \frac{1}{2}\sum_{i=1}^{N} n_i} d\gamma \Big] dn_i \Bigg] \quad (11)$$

Finally, using the integral $\int_0^{\infty} e^{-b\gamma} \gamma^{-\frac{1}{2} - \frac{1}{2}\sum_{i=1}^{N} n_i} d\gamma = b^{-\frac{1}{2} + \frac{1}{2}\sum_{i=1}^{N} n_i} \Gamma(\frac{1}{2} - \frac{1}{2}\sum_{i=1}^{N} n_i)$ in (11) with the definition of N-multivariate Fox's H function [28, A.1], we get:

$$\bar{P}_e = \Big(a\sqrt{\frac{1}{4\pi}} \prod_{i=1}^{N} \prod_{j=1}^{2} \psi_{i,j} \zeta_{i,j}^{-\frac{\phi_{i,j}}{\alpha_{i,j}}} \Big) \times H_{1,1:3,4;\cdots;3,4}^{0,1:4,1;\cdots;4,1} \Bigg[U(\gamma_0) \Bigg| \begin{matrix} (\frac{1}{2}; \frac{1}{2}, \cdots, \frac{1}{2}) : V_1 \\ (0; 1, \cdots, 1) : V_2 \end{matrix} \Bigg] \quad (12)$$

where $U(\gamma_0) = \{\sqrt{\frac{1}{b\gamma_0}} \prod_{j=1}^{2} \zeta_{i,j}^{\frac{1}{\alpha_{i,j}}}\}_{i=1}^{N}$, $V_1 = \{(1,1), \{(1+\phi_{i,j}, 1)\}_1^2\}_{i=1}^{N}$, and $V_2 = \{\{(\mu_{1,j}, \frac{1}{\alpha_{i,j}})\}_1^2, \{(\phi_{i,j}, 1)\}_1^2\}_{i=1}^{N}$.

Similar to the outage probability, an asymptotic expression of the average BER $\bar{P}_e^{\infty}$ at high SNR $\gamma_0 \to \infty$:

$$\bar{P}_e \approx \bar{P}_e^{\infty} = a\sqrt{\frac{1}{4\pi}} \prod_{i=1}^{N} \prod_{j=1}^{2} \psi_{i,j} \zeta_{i,j}^{-\frac{\phi_{i,j}}{\alpha_{i,j}}} \Big(\sqrt{\frac{1}{b\gamma_0}} \prod_{j=1}^{2} \zeta_{i,j}^{\frac{1}{\alpha_{i,j}}} \Big)^{p_i - 1} \Gamma\Big(\frac{1}{2} + \frac{1}{2}\sum_{i=1}^{N} p_i\Big) \Gamma(p_i) \times \frac{\prod_{j=1, \mu_{i,j} \neq \frac{p_i}{\alpha_{i,j}}}^{2} \Gamma(\mu_{i,j} - \frac{p_i}{\alpha_{i,j}}) \prod_{j=1, \phi_{i,j} \neq p_i}^{2} \Gamma(\phi_{i,j} - p_i)}{\Gamma(1 + \sum_{i=1}^{N} p_i) \prod_{j=1}^{2} \Gamma(1 + \phi_{i,j} - p_i)} \quad (13)$$

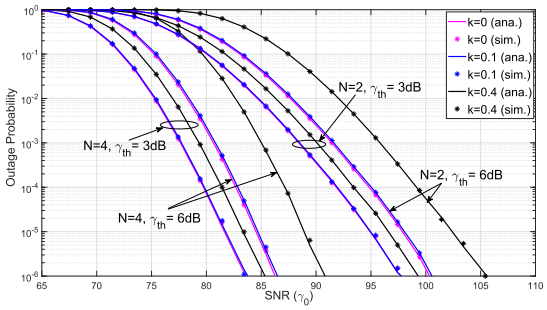

Fig. 1. Impact of transceiver impairments.

where $p_i = \min\{\alpha_{i,1}\mu_{i,1}, \phi_{i,1}, \alpha_{i,2}\mu_{i,2}, \phi_{i,2}\}$. Expressing (13) as $\bar{P}_e^{\infty} \propto \gamma_0^{-G_{\text{BER}}}$, we get the BER-diversity order as $G_{\text{BER}} = \sum_{i=1}^{N} \min\{\frac{\alpha_{i,1}\mu_{i,1}-1}{2}, \frac{\phi_{i,1}-1}{2}, \frac{\alpha_{i,2}\mu_{i,2}-1}{2}, \frac{\phi_{i,2}-1}{2}\}$. Similar to the outage probability, we show analytically that the average BER performance increases with N at high SNR by simplifying (13) for the i.i.d. case with $\phi > \alpha\mu$

$$\bar{P}_e^{\infty} = \frac{a}{\sqrt{4\pi b}} \frac{\mu^{-2/\alpha}}{\Omega^{-2} S^{-2}} \frac{\Gamma\Big(\frac{1}{2} + \frac{N}{2}\alpha\mu\Big)}{\Gamma(1+N\alpha\mu)} \times \Bigg[\Big(\frac{1}{b\Omega^4 S^4 \gamma_0} \Big)^{\frac{\alpha\mu-1}{2}} \frac{\alpha\phi^2 \mu^{\frac{2(\alpha\mu-1)}{\alpha}} \Gamma(\alpha\mu)}{(\phi-\alpha\mu)^2 (\Gamma(\mu))^2} \Bigg]^N \quad (14)$$

3) Ergodic Capacity: For a slow-fading THz channel, the ergodic capacity is:

$$\bar{\eta} = \log_2(e) \int_0^{\infty} \ln(1+\gamma) f_{\gamma}(\gamma) d\gamma \quad (15)$$

We substitute $f_{\gamma}(\gamma)$ from (6) with $k=0$ in (15), apply the definition of Multivariate Fox's H function with $\ln(1+\gamma) = \frac{1}{2\pi\jmath} \int_{\mathcal{L}} \frac{\Gamma(u+1)\Gamma(-u)^2}{\Gamma(1-u)} (\gamma)^{-u} du$ to solve the resultant inner integral $I = \frac{1}{2\pi\jmath} \int_{\mathcal{L}} \frac{\Gamma(u+1)\Gamma(-u)^2}{\Gamma(1-u)} \epsilon^{u+\frac{1}{2}\sum_{i=1}^{N} n_i} \Gamma\big(-u - \frac{1}{2}\sum_{i=1}^{N} n_i\big) du$ using the final value theorem $\lim_{x\to\infty} \int_0^x f(u)\, du = \lim_{s\to 0} F(s) = F(\epsilon)$, where ϵ is close to zero (in the order 10^{-7}) to get:

$$\bar{\eta} = \Big(\frac{\log_2(e)}{2} \prod_{i=1}^{N} \prod_{j=1}^{2} \psi_{i,j} \zeta_{i,j}^{-\frac{\phi_{i,j}}{\alpha_{i,j}}} \Big) \times H_{1,1:3,4;\cdots;3,4;2,2}^{0,1:4,1;\cdots;4,1;1,2} \Bigg[U(\gamma_0) \Bigg| \begin{matrix} (1; \frac{1}{2}, \ldots, \frac{1}{2}, 1) : V_1 \\ (1; 1, \cdots, 1, 0) : V_2 \end{matrix} \Bigg] \quad (16)$$

where $U(\gamma_0) = \{\{\sqrt{\frac{1}{\epsilon\gamma_0}} \prod_{j=1}^{2} \zeta_{i,j}^{\frac{1}{\alpha_{i,j}}}\}_{i=1}^{N}, \frac{1}{\epsilon}\}$, $V_1 = \{\{(1,1), \{(1+\phi_{i,j}, 1)\}_1^2\}_{i=1}^{N}; (1,1), (1,1)\}$ and $V_2 = \{\{\{(\mu_{1,j}, \frac{1}{\alpha_{i,j}})\}_1^2, \{(\phi_{i,j}, 1)\}_1^2\}_{i=1}^{N}; (1,1), (0,1)\}$.

V. Simulation and Numerical Results

In this section, we demonstrate the impact of RIS elements on THz wireless transmissions. We consider THz carrier frequency $f = 300$GHz, antenna gains $G = 40$dBi, and molecular absorption coefficient $k = 3.18 \times 10^{-4}$ per meter. We consider the near-field broadcasting model [25] to compute the path-gain using the formula $h_l = \frac{cG}{4\pi f(d_1+d_2)} \exp(-\frac{1}{2}k(d_1+d_2))$, where $d_1 = 5$m and $d_2 = 25$m are the distances from the source to the RIS and the RIS to the destination,

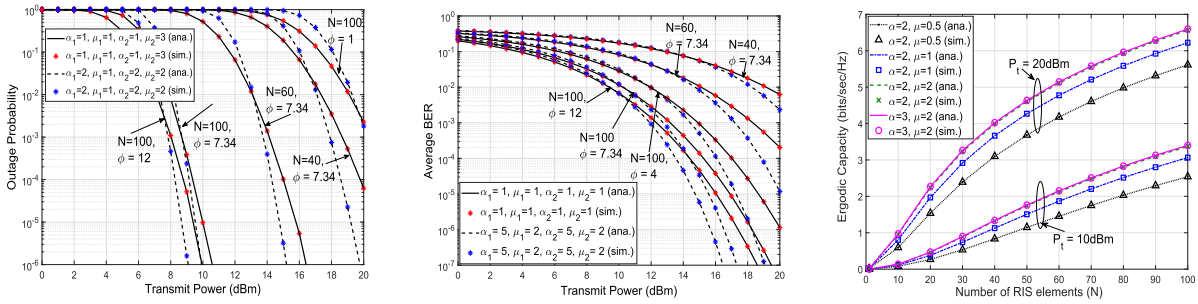

(a) Outage probability. (b) Average BER. (c) Ergodic capacity.

Fig. 2. RIS-THz performance for various pointing errors and fading scenarios without hardware impairments $k = 0$.

respectively. We consider i.ni.d and i.i.d fading parameters for both the paths; however, the same parameters for each RIS element using α-μ and pointing errors distributions. We use the pointing errors model of [29] to compute S_i and ϕ_i, $\forall i$. A noise floor of -74dBm is considered over a 10GHz channel bandwidth. Under certain scenarios, a lower signal bandwidth can be considered with a reduced noise power to ensure flat fading. We also validate our derived analytical expressions with Monte Carlo simulations (averaged over 10^8 channel realizations) and numerical analysis (using Python code implementation of multivariable Fox's H function [30]). In all simulation plots, we denote "ana." as the numerical evaluation of derived analytical expressions of multi-variate Fox's H function, and "sim." as the Monte Carlo simulations.

In Fig. 1, we demonstrate the impact of hardware impairments on the outage probability by considering different threshold SNR γ_{th} and RIS elements. It can be seen that there is an increase in the outage probability when the hardware impairment factor $k > 0.1$. Moreover, the impact of hardware imperfections becomes severe for higher threshold SNR γ_{th} since the transceiver impairments limit the peak SNR within $1/k^2$. However, the use of RIS improves outage performance. In Fig. 2(a), we illustrate the impact of RIS elements on the outage probability of RIS-THz transmissions for various fading and pointing errors scenarios with negligible hardware impairments and $\gamma_{\text{th}} = 6$dB. Considering Rayleigh fading ($\alpha_1 = 2$, $\mu_1 = 1$) in the first path and Nakagami-2 fading ($\alpha_2 = 2$, $\mu_2 = 2$) in the second path, the figure shows a gain of approximately 10dBm in the transmit power when the number of RIS elements is increased from $N = 40$ to $N = 100$ for an outage probability of 10^{-4} at $\phi = 7.34$. A similar trend can be observed when the simulation experiments are repeated for the Weibull fading ($\alpha_1 = 1$, $\mu_1 = 1$) and the Gamma fading ($\alpha_2 = 1$, $\mu_2 = 3$). Comparing the slopes for $N = 100$ at different ϕ, it can be observed that the diversity order becomes independent of pointing errors when $\phi = 7.34$ or $\phi = 12$ since $\phi > \alpha_1\mu_1 = 1$ and $\phi > \alpha_2\mu_2 = 2$.

Fig. 2(b) depicts the average BER for QPSK modulation ($a = 1$, $b = 1/4$) for the THz-RIS wireless system with i.i.d fading models We consider two fading scenarios: ($\alpha = 1$, $\mu = 1$) and ($\alpha = 5$, $\mu = 2$) for various pointing errors to demonstrate the effect of fading and number of RIS elements on the average BER. It can be seen from the figure that the RIS provides significant savings in transmit power to achieve the same BER. Further, comparing the slopes of Fig. 2(a) and Fig. 2(b), it can be inferred that diversity order is higher for the outage probability than those obtained from the asymptotic average BER expression. The impact of fading and pointing error parameters on diversity order can be observed for $N = 100$ with ϕ comparing the dotted lines with thick lines depicting two fading scenarios. It can be seen that the diversity order is limited by the pointing errors when $\phi < \alpha_2\mu_2 = 10$. However, diversity order of the system is determined by the fading parameters when $\phi > \alpha_1\mu_1 = 1$.

Finally, we demonstrate the ergodic capacity versus the number of RIS elements at two different transmit powers 10dBm and 20dBm for different α-μ parameters assuming i.i.d fading in two paths at $\phi = 7.34$, as shown in Fig. 2(c). We can make two important observations among others. The ergodic capacity increases almost linearly for a lower value of N and logarithmic for a higher value of N. Further, for a fixed α, the performance of RIS-THz system improves with an increase in μ for a given N. Similarly, the figure shows that there is a gain in the performance for a given μ and N when α increases.

VI. Conclusion

We presented an exact analysis of the performance of RIS-empowered THz wireless transmissions over α-μ with pointing errors. The derived closed-form expressions of outage probability, average BER, and ergodic capacity show the impact of RIS elements on the performance of considered system. Asymptotic analysis of outage probability and average BER was developed to derive the diversity order of the system, which showed design specifications to mitigate the impact of pointing errors and performance improvement with an increase in the number of RIS elements. Simulation results were presented to validate the mathematical insights over various fading configurations of interests. The RIS significantly improves the performance of THz wireless transmissions when the direct path does not exist by controlling the phase of the reflected signals, thereby creating a virtual line-of-sight path. The proposed research can be extended with cooperative relaying, consideration of imperfect/random phase information, and correlated fading at the RIS.

Appendix A
MGF of Z_i

We use the Mellin transform to represent the PDF of Z_i

$$f_{Z_i}(z) = \frac{z^{-1}}{2\pi\jmath}\int_{\mathcal{L}}\prod_{j=1}^{L}\int_0^\infty \psi_j r^{n+\phi_j-1} \times\Gamma\Big(\mu_j - \frac{\phi_j}{\alpha_j}, \zeta_j r^{\alpha_j}\Big) dr z_i^{-n} dn \quad (17)$$

where the inner integral denotes the n-th moment of h_i (see (2)). Substituting $r^{\alpha_j} = p$ in (17) with the identities [[31], 6.455/1] and $\prod_{j=1}^{L} \frac{1}{\phi_j+n} = \prod_{j=1}^{L} \frac{\Gamma(\phi_j+n)}{\Gamma(\phi_j+n+1)}$ [31, 8.331.2]:

$$f_{Z_i}(z) = \frac{1}{z}\frac{1}{2\pi\jmath}\prod_{j=1}^{L}\psi_j\zeta_j^{-\frac{\phi_j}{\alpha_j}}\int_{\mathcal{L}}\prod_{j=1}^{L}\frac{\Gamma(\phi_j+n)}{\Gamma(\phi_j+n+1)} \times\prod_{j=1}^{L}\Gamma\big(\mu_j+\frac{n}{\alpha_j}\big)\Big(\frac{1}{z}\prod_{j=1}^{L}\zeta_j^{\frac{-1}{\alpha_j}}\Big)^n dn \quad (18)$$

Using the definition of the MGF, we get

$$M_{Z_i}(s) = \int_0^\infty \frac{1}{z}\prod_{j=1}^{L}\psi_j\zeta_j^{-\frac{\phi_j}{\alpha_j}}\frac{1}{2\pi\jmath}\int_{\mathcal{L}}\prod_{j=1}^{L}\frac{\Gamma(\phi_j+n)}{\Gamma(\phi_j+n+1)} \times\prod_{j=1}^{L}\Gamma\big(\mu_j+\frac{n}{\alpha_j}\big)\Big(\frac{1}{z}\prod_{j=1}^{L}\zeta_j^{\frac{-1}{\alpha_j}}\Big)^n dn e^{-sz}dz \quad (19)$$

Interchanging the order of integration, $\int_0^\infty e^{-sz}z^{-n-1}dz = s^n\Gamma(-n)$, and applying the definition of Fox's H function [28, A.1], we get (3).

APPENDIX B
PDF AND CDF OF Z

Using definition of the MGF function, we can apply the inverse Laplace transform to find the PDF of $Z = \sum_{i=1}^{N} Z_i$ as $f_Z(z) = \mathcal{L}^{-1}\prod_{i=1}^{N} M_{Z_i}(s)$. Thus, using (3) and interchanging the order of integration, we get

$$f_Z(z) = \prod_{i=1}^{N}\prod_{j=1}^{L}\psi_{i,j}\zeta_{i,j}^{-\frac{\phi_{i,j}}{\alpha_{i,j}}}\Big[\frac{1}{(2\pi\jmath)^N}\int_{\mathcal{L}}\prod_{j=1}^{L}\frac{\Gamma(\phi_{i,j}+n_i)\Gamma(-n_i)}{\Gamma(\phi_{i,j}+n_i+1)} \times\prod_{j=1}^{L}\Gamma\big(\mu_{i,j}+\frac{n_i}{\alpha_{i,j}}\big)\Big(\prod_{j=1}^{L}\zeta_{i,j}^{\frac{-1}{\alpha_{i,j}}}\Big)^{n_i} \times\left(\frac{1}{2\pi\jmath}\int_{\mathcal{L}} s^{\sum_{i=1}^{N} n_i}e^{sz}ds\right)dn_i\Big] \quad (20)$$

We apply [31, 8.315.1] to solve the inner integral in (20) as

$$\int_{\mathcal{L}} s^{\sum_{i=1}^{N} n_i}e^{sz}ds = \left(\frac{1}{z}\right)^{1+\sum_{i=1}^{N} n_i}\frac{2\pi\jmath}{\Gamma(-\sum_{i=1}^{N} n_i)} \quad (21)$$

Using (21) in (20) and applying the definition of N-Multivariate Fox's H function in [28, A.1], we get (4). To derive the CDF, we use $F_Z(z) = \mathcal{L}^{-1}\prod_{i=1}^{N}\frac{M_{Z_i}(s)}{s}$ and apply the similar steps used in the derivation of PDF to get (5).

REFERENCES

[1] M. D. Renzo *et al.*, "Smart radio environments empowered by reconfigurable AI meta-surfaces: An idea whose time has come," *EURASIP J. Wireless Commun. Netw.*, vol. 2019, no. 1, Dec. 2019, Art. no. 129.

[2] E. Basar *et al.*, "Wireless communications through reconfigurable intelligent surfaces," *IEEE Access*, vol. 7, pp. 116753–116773, 2019.

[3] Q. Wu *et al.*, "Intelligent reflecting surface aided wireless communications: A tutorial," *IEEE Trans. Commun.*, vol. 69, no. 5, pp. 3313–3351, May 2021.

[4] S. Koenig *et al.*, "Wireless sub-THz communication system with high data rate," *Nature Photon.*, vol. 7, no. 12, pp. 977–981, Dec. 2013.

[5] A. Alexiou *et al.*, "THz communications: A catalyst for the wireless future," *IEEE Commun. Mag.*, vol. 58, no. 11, pp. 12–13, Nov. 2020.

[6] D. Kudathanthirige *et al.*, "Performance analysis of intelligent reflective surfaces for wireless communication," in *Proc. IEEE Int. Conf. Commun. (ICC)*, Jun. 2020, pp. 1–6.

[7] A. A. A. Boulogeorgos and A. Alexiou, "Ergodic capacity analysis of reconfigurable intelligent surface assisted wireless systems," in *Proc. IEEE 3rd 5G World Forum (5GWF)*, Sep. 2020, pp. 395–400.

[8] A.-A.-A. Boulogeorgos and A. Alexiou, "Performance analysis of reconfigurable intelligent surface-assisted wireless systems and comparison with relaying," *IEEE Access*, vol. 8, pp. 94463–94483, 2020.

[9] L. Yang *et al.*, "Accurate closed-form approximations to channel distributions of RIS-aided wireless systems," *IEEE Wireless Commun. Lett.*, vol. 9, no. 11, pp. 1985–1989, Nov. 2020.

[10] Q. Tao *et al.*, "Performance analysis of intelligent reflecting surface aided communication systems," *IEEE Commun. Lett.*, vol. 24, no. 11, pp. 2464–2468, Nov. 2020.

[11] R. C. Ferreira *et al.*, "Bit error probability for large intelligent surfaces under double-Nakagami fading channels," *IEEE Open J. Commun. Soc.*, vol. 1, pp. 750–759, 2020.

[12] D. Selimis *et al.*, "On the performance analysis of RIS-empowered communications over Nakagami-m fading," *IEEE Commun. Lett.*, vol. 25, no. 7, pp. 2191–2195, Jul. 2021.

[13] H. Ibrahim *et al.*, "Exact coverage analysis of intelligent reflecting surfaces with Nakagami-M channels," *IEEE Trans. Veh. Technol.*, vol. 70, no. 1, pp. 1072–1076, Jan. 2021.

[14] H. Du *et al.*, "Millimeter wave communications with reconfigurable intelligent surfaces: Performance analysis and optimization," *IEEE Trans. Commun.*, vol. 69, no. 4, pp. 2752–2768, Apr. 2021.

[15] L. Kong *et al.*, "Effective rate evaluation of RIS-assisted communications using the sums of cascaded α-μ random variates," *IEEE Access*, vol. 9, pp. 5832–5844, 2021.

[16] I. Trigui *et al.*, "A comprehensive study of reconfigurable intelligent surfaces in generalized fading," 2020, *arXiv:2004.02922*. [Online]. Available: http://arxiv.org/abs/2004.02922

[17] H. Sarieddeen *et al.*, "Terahertz-band ultra-massive spatial modulation MIMO," *IEEE J. Sel. Areas Commun.*, vol. 37, no. 9, pp. 2040–2052, Jul. 2019.

[18] K. Dovelos *et al.*, "Intelligent reflecting surfaces at terahertz bands: Channel modeling and analysis," in *Proc. IEEE Int. Conf. Commun. Workshops (ICC Workshops)*, Jun. 2021, pp. 1–6.

[19] C. Huang *et al.*, "Multi-hop RIS-empowered terahertz communications: A DRL-based hybrid beamforming design," *IEEE J. Sel. Areas Commun.*, vol. 39, no. 6, pp. 1663–1677, Jun. 2021.

[20] H. Du *et al.*, "Reconfigurable intelligent surface aided TeraHertz communications under misalignment and hardware impairments," 2020, *arXiv:2012.00267*. [Online]. Available: http://arxiv.org/abs/2012.00267

[21] A.-A.-A. Boulogeorgos and A. Alexiou, "Error analysis of mixed THz-RF wireless systems," *IEEE Commun. Lett.*, vol. 24, no. 2, pp. 277–281, Feb. 2020.

[22] P. Bhardwaj and S. M. Zafaruddin, "Performance of dual-hop relaying for THz-RF wireless link," in *Proc. IEEE 93rd Veh. Technol. Conf. (VTC-Spring)*, Apr. 2021, pp. 1–5.

[23] E. N. Papasotiriou *et al.*, "A new look to THz wireless links: Fading modeling and capacity assessment," in *Proc. IEEE 32nd Annu. Int. Symp. Pers., Indoor Mobile Radio Commun.*, Jun. 2021, pp. 1–6.

[24] A.-A.-A. Boulogeorgos and A. Alexiou, "How much do hardware imperfections affect the performance of reconfigurable intelligent surface-assisted systems?" *IEEE Open J. Commun. Soc.*, vol. 1, pp. 1185–1195, 2020.

[25] W. Tang *et al.*, "Wireless communications with reconfigurable intelligent surface: Path loss modeling and experimental measurement," *IEEE Trans. Wireless Commun.*, vol. 20, no. 1, pp. 421–439, Jan. 2021.

[26] G. C. Alexandropoulos and P. T. Mathiopoulos, "Performance evaluation of selection diversity receivers over arbitrarily correlated generalised gamma fading channels," *IET Commun.*, vol. 4, no. 10, p. 1253, 2010.

[27] Y. A. Rahama *et al.*, "On the sum of independent Fox's H-function variates with applications," *IEEE Trans. Veh. Technol.*, vol. 67, no. 8, pp. 6752–6760, Aug. 2018.

[28] A. Mathai *et al.*, *The H-Function: Theory and Applications*. New York, NY, USA: Springer, 2009.

[29] A. A. Farid and S. Hranilovic, "Outage capacity optimization for free-space optical links with pointing errors," *J. Lightw. Technol.*, vol. 25, no. 7, pp. 1702–1710, Jul. 2007.

[30] H. R. Alhennawi *et al.*, "Closed-form exact and asymptotic expressions for the symbol error rate and capacity of the H-function fading channel," *IEEE Trans. Veh. Technol.*, vol. 65, no. 4, pp. 1957–1974, Apr. 2016.

[31] I. Gradshteuin *et al.*, *Table of Integrals, Series, and Products*, 7th ed. New York, NY, USA: Academic, 2007.